AFRL-HE-WP-TP-2006-0047

AIR FORCE RESEARCH LABORATORY

Statistical Assessment of NVG Noise

Jesse G. Wales
Peter L. Marasco

Human Effectiveness Directorate
Warfighter Interface Division
Wright-Patterson AFB OH 45433-7022

March 2006

20060403504

Human Effectiveness Directorate
Warfighter Interface Division
Wright-Patterson AFB OH 45433

REPORT DOCUMENTATION PAGE

1. REPORT DATE (DD-MM-YYYY) March 2006	2. REPORT TYPE Technical Paper		3. DATES COVERED (From - To)
4. TITLE AND SUBTITLE Statistical Assessment of NVG Noise			**5a. CONTRACT NUMBER**
			5b. GRANT NUMBER
			5c. PROGRAM ELEMENT NUMBER
6. AUTHOR(S) Jesse G. Wales, Peter L. Marasco			**5d. PROJECT NUMBER** 7184
			5e. TASK NUMBER 11
			5f. WORK UNIT NUMBER 27
7. PERFORMING ORGANIZATION NAME(S) AND ADDRESS(ES) AND ADDRESS(ES)			**8. PERFORMING ORGANIZATION REPORT NUMBER**
9. SPONSORING / MONITORING AGENCY NAME(S) AND ADDRESS(ES) Air Force Materiel Command Air Force Research Laboratory Human Effectiveness Directorate Warfighter Interface Division Wright-Patterson AFB OH 45433-7022			**10. SPONSOR/MONITOR'S ACRONYM(S)** AFRL/HECV **11. SPONSOR/MONITOR'S REPORT NUMBER(S)** AFRL-HE-WP-TP-2006-0047

12. DISTRIBUTION / AVAILABILITY STATEMENT

Approved for public release; distribution is unlimited.

13. SUPPLEMENTARY NOTES

This will be published in the Proceedings of the SPIE Defense & Security Symposium Conference. The clearance number is AFRL/WS-06-0632, cleared 8 March 2006.

14. ABSTRACT

New advancements in charged-coupled device (CCD) technology allow for further investigation into the spatial nature of night vision goggle (NVG) noise distributions. This is significant because it is common practice in new NVG technology to combine image intensifiers with CCDs for night vision imaging. In this study, images of NVG noise are recorded by a CCD camera while varying input radiance and using multiple goggle types. Noise distributions characterized using histograms of these images are analyzed and fitted with curves. Using the changes in the distribution and relating distribution changes (coefficient changes) to input radiance and goggle performance provides a very accurate noise characterization. This study finds that a Weibull distribution seems more appropriate than a Poisson distribution, producing higher correlation coefficient fits. In addition, the paper suggests possible ways the noise models developed here can impact advancements in NVG image enhancement using this new technology.

15. SUBJECT TERMS

Night vision, goggle, NVG, noise, image intensifier, CCD, histogram, Weibull

16. SECURITY CLASSIFICATION OF:			17. LIMITATION OF ABSTRACT	18. NUMBER OF PAGES	19a. NAME OF RESPONSIBLE PERSON Jesse G. Wales
a. REPORT UNC	b. ABSTRACT UNC	c. THIS PAGE UNC	SAR	22	19b. TELEPHONE NUMBER (include area code) (937) 255-8361

Statistical Assessment of Night Vision Goggle Noise

Jesse G. Wales and Peter L. Marasco
Air Force Research Laboratory, Battlespace Visualization Branch,
2255 H Street, Wright-Patterson AFB, OH 45433-7022

ABSTRACT

New advancements in charged-coupled device (CCD) technology allow for further investigation into the spatial nature of night vision goggle (NVG) noise distributions. This is significant because it is common practice in new NVG technology to combine image intensifiers with CCDs for night vision imaging. In this study, images of NVG noise are recorded by a CCD camera while varying input radiance and using multiple goggle types. Noise distributions characterized using histograms of these images are analyzed and fitted with curves. Using the changes in the distribution and relating distribution changes (coefficient changes) to input radiance and goggle performance provides a very accurate noise characterization. This study finds that a Weibull distribution seems more appropriate than a Poisson distribution, producing higher correlation coefficient fits. In addition, the paper suggests possible ways the noise models developed here can impact advancements in NVG image enhancement using this new technology.

Keywords: night vision, goggle, NVG, noise, image intensifier, I^2, CCD, histogram, Weibull,

1. INTRODUCTION

Anecdotal evidence seems to suggest that NVGs of different types and ages have different perceived noise characteristics. There are two main perceived characteristics of NVG noise. First, the graininess of an NVG image is due to the variance in arrival times of photons at low light levels. Second, random and bright point flashes of light known as scintillations, "poppers"[1], or "sparkle"[2], are caused by residual gas and out-gassing within the image intensifier (I^2) tube[2]. Recently, computer simulations of the various noise characteristics were used to subjectively assess the noise differences between goggles and input light levels. But variability between subjects did not allow for quantifiable results[1]. Also, these studies suggested that people may perceive NVG noise differently and that the characteristics of NVG noise may be weighted differently from subject to subject.[3,4] The origins of these perceptual differences was unclear. Furthermore, these studies seemed to indicate that NVGs exhibit unique noise characteristics and are dependant on input light levels.

1.1. Noise and Combinations of Noise Mechanisms

Theoretically speaking, the most basic noise mechanism found in electro-optical systems in photon noise, which can be described using a Poissonian statistical distribution. However, to get a more accurate description of sensor noise, one must include a number of non-Poissionian mechanisms. To combine noise, mathematically speaking, one calculates the root mean square of the contributions. This process can lead to noise characteristics that are decidedly non-Poissionian, depending on the nature and strength of the different contributions.[6]

The literature seems to indicate that most, but not all, noise mechanisms in the image intensifier tube can be statistically described using the Poissionian distribution. NVG noise is generally regarded to be Poissionian in nature. However, research indicted that a number of mechanisms within the image intensifer tube are non-Poissionian. For example, the probability of an electron entering a microchannel is considered best described by a binomial distribution.[7] Also, noise resulting from secondary electron generation is considered essentially Poissionian, but not purely Poissionian.[7] In addition, the Poission distribution is believed to not well predict some NVG noise characteristics including the scintillations inherent in NVGs, due in part to residual gas and ions within the I^2 tube. The combination of these factors seems to suggest that image intensifier tube noise statistics may be Poissionian in nature but might not necessarily be purely Poissionian.

1.2. Poisson vs. Weibull

Multiple papers have examined ways to classify NVG noise using both subjective and objective means.[1,2,3,4,7] Many methods have been used to determine signal to noise ratio, photon probability distribution, scintillation gain/frequency/density, modulation transfer function, etc. in efforts to quantify image intensifier tube noise. Early models of noise used photomultiplier tubes to study the temporal nature of intensifier noise. The spatial nature of I^2 tube noise and its interaction with solid state imagers is a current topic of interest to the industry. In order to study the spatial characteristics of NVG noise, it is theorized that a sensitive CCD camera could be used to capture images through the NVG of a uniform field of known radiance. Histograms of these images are used to attempt to characterize the noise of multiple goggles under several conditions (such as input radiance, filters, and eyepiece diopter setting). The histograms are studied by fitting a Weibull distribution curve to the data.

A Weibull distribution (Equation 1) was fit to the histogram curves generating Weibull coefficients (A, B, C, and D). Since we were trying to characterize electro-optical sensor noise, noises known to be generally Poissionian in nature, the obvious choice of statistical distribution was the Poissionian (Equation 2). However, the curve fitting software used here did not allow for automatic fitting of the Poissionian distribution and higher goodness-of-fit R^2 values were achieved by automatic fitting of the Weibull distribution. Additionally, the Poissionian curve can be represented very well by a Weibull distribution (achieving R^2 values greater than 0.999) as shown in Figure 1 below. Therefore, the authors chose to analyze the noise histograms using the Weibull. The Weibull has four coefficients that are tailored to each histogram. The first two Weibull coefficients, A and B, describe the curve's peak amplitude and peak location (average gray level), respectively. The last two Weibull coefficients, C and D, together describe the curve's shape such as width and slop steepness on the front and back side of the curve. As the C coefficient increases, the curve will become wider and the back side will be more rounded. As the D coefficient increases, the curve will become narrower and the front side of the curve will be more rounded.

$$f_w(x) = A\left(\frac{D-1}{D}\right)^{\frac{1-D}{D}}\left[\frac{x-B}{C}+\left(\frac{x-B}{C}\right)^{\frac{1}{D}}\right]^{D-1}\exp\left[-\left(\frac{x-B}{C}+\left(\frac{D-1}{D}\right)^{\frac{1}{D}}\right)^D+\frac{D-1}{D}\right] \qquad (1)$$

$$f_p(x) = A\frac{e^{-a}a^x}{(x)!} \qquad (2)$$
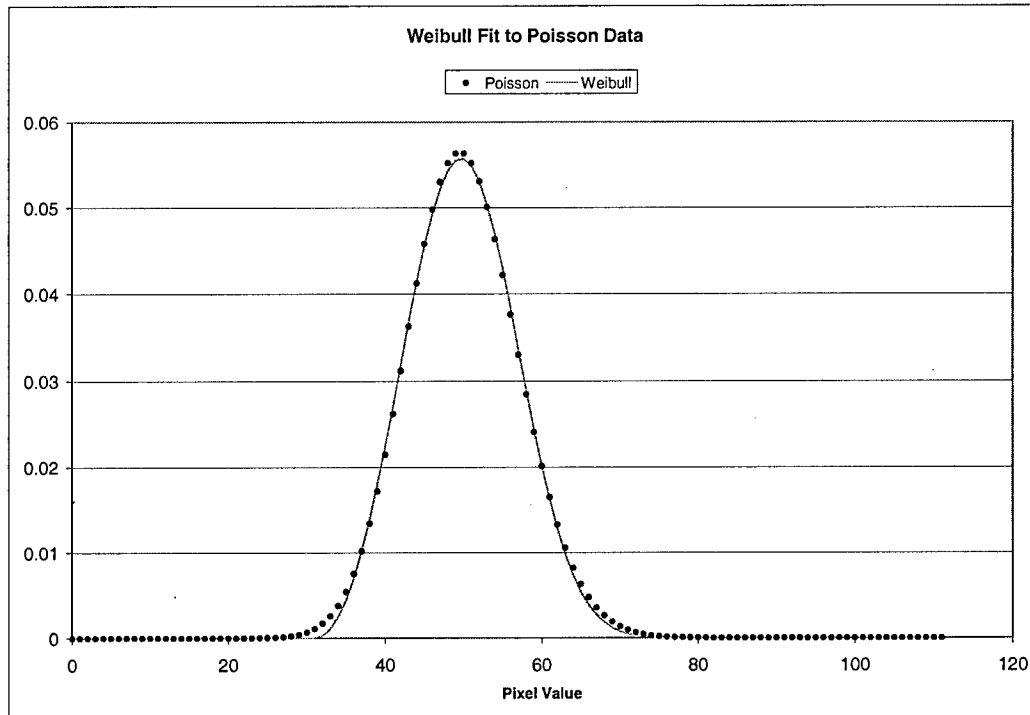
Figure 1. Weibull distribution fit to Poisson generated data.

The study performed in this paper will attempt to reconcile theory and perception by taking the subjective user out of the equation and replace them with a digital camera in order to quantify any possible noise differences. In addition to varying the input light, other variables such as minus blue filter and eyepiece setting will be examined to see if they contribute a quantifiable difference in NVG noise.

2. PROCEDURE

The general procedure was to illuminate one channel of a night vision goggle with a uniform field of known radiance and then capture an image using a digital camera in the place of a human eye (see Figure 2-Setup image). A histogram of the image pixel values was then taken and a Weibull curve fit to the histogram. Finally, the Weibull coefficients were compared for each of the varying parameters. The parameters of importance in this paper include: input radiance, NVG type, varying filters, and eyepiece diopter setting.

The experimental setup is illustrated by Figure 2 below. A uniform field was created using a large box lined with white poster board, referred to from this point forward in this paper as "the LED box." This box is described in detail in the paper "Psychophysical measurement of night vision goggle noise" by Glascow, et al[1]. One side of the LED box has a port cut for the NVG to look through. Surrounding the NVG port on the inside of the LED box are four infrared light emitting diodes (LEDs) with adjustable voltage. A spectroradiometer was used to correlate LED voltage to NVIS_B radiance. One channel of an NVG was focused on the back of the inside of the LED box using a temporary focusing target. For all conditions except the eyepiece magnification study, the eyepiece was set to -1.0 diopters. This setting was chosen for two reasons. First, this aided in the focusing of the camera lens. Second, studies have shown that on average NVG users tend to select about -1 diopters.[8] After the NVG was focused on the back of the LED box, a CCD digital camera was positioned behind the NVG eyepiece. This camera was then focused through the NVG onto the back of the LED box. The camera was positioned as close as possible to the NVG eyepiece and centered on the bright spot of the NVG image (the bright spot can be seen easily by adjusting the image contrast and gain of the camera). The focusing target was then removed.

Camera parameters were chosen to emulate the human eye as well as one could with the available equipement. Therefore, a pixel field of view of one minute of arc or better and a shutter speed equal to or faster then 1/30 sec were desired. The available CCD camera had a 1000x1000 square pixel format, with square pixels, 4.75 microns on a side, and 10-bit grey scale. To achieve the desired resolution, a 50 mm lens set to f/2.6 was mated to the camera. Shutter speed was chosen to be 1/50 sec. The CCD was set to run in two by two binning mode to increase sensitivity. With this setup, there was a pixel field of view of 0.64 minutes of arc.
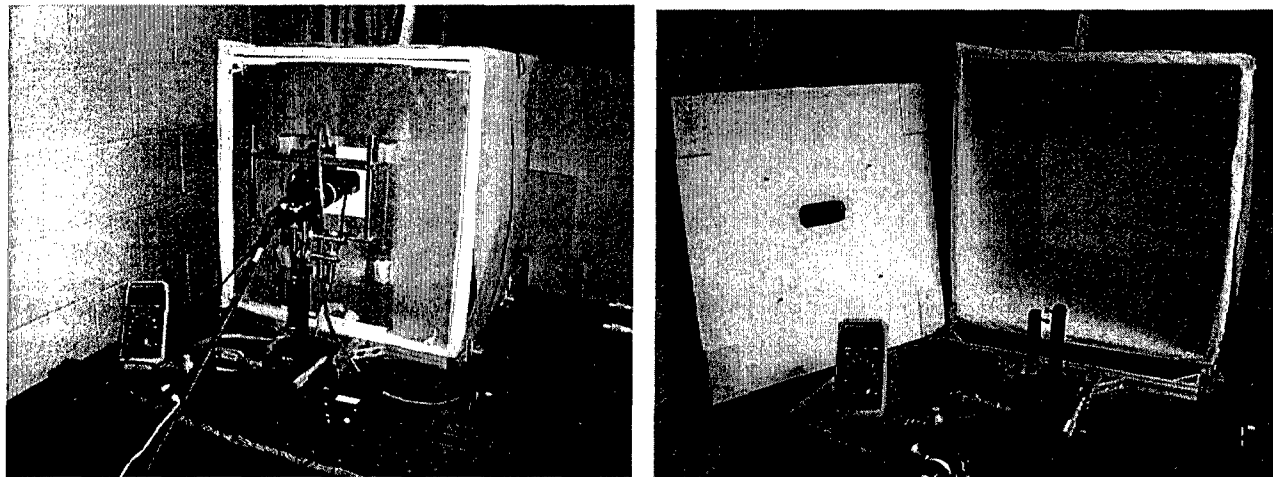

Figure 2. Experiment setup. Digital camera on output of NVG looking into 'LED box'

Before data collection began, an appropriate range of radiance inputs was found. For this task, the goggle output was measured for the full range of radiance inputs. The camera was removed and a photometer with an interface specifically designed to measure NVG output luminance was used[5]. A plot of goggle output luminance versus radiance input, Figure 3, was used to select the input radiances used in the study. Four radiances were selected. One radiance corresponds to a low goggle output. The second corresponds to a middle goggle output. The third corresponds to the beginning of the auto-gain level (where the auto-gain feature of the goggles limits the output). The fourth corresponds to a radiance well beyond the point where the auto-gain limits the output. The radiances chosen were $4.6E-11$ W/cm^2sr, $6.1E-10$ W/cm^2sr, $2.8E-9$ W/cm^2sr, and $9.2E-8$ W/cm^2sr, which roughly correspond to one third "starlight" ($1.58E-10$ W/cm^2sr), "quarter moon" ($5.6E-10$ W/cm^2sr), "full moon" ($2.92E-09$ W/cm^2sr), and 30 times "full moon", respectively (using values described by the Hoffman LM-33-80A)[9]. The choices of input radiances was made in order to examine NVG noise under several conditions. The conditions included a very low input, a moderate input, an input that is just large enough to invoke the auto-gain feature of the goggles, and an extremely large input to study the effects of NVG noise under high input. Note that the AN/AVS-6 has a significantly lower output than the AN/AVS-9 goggles.
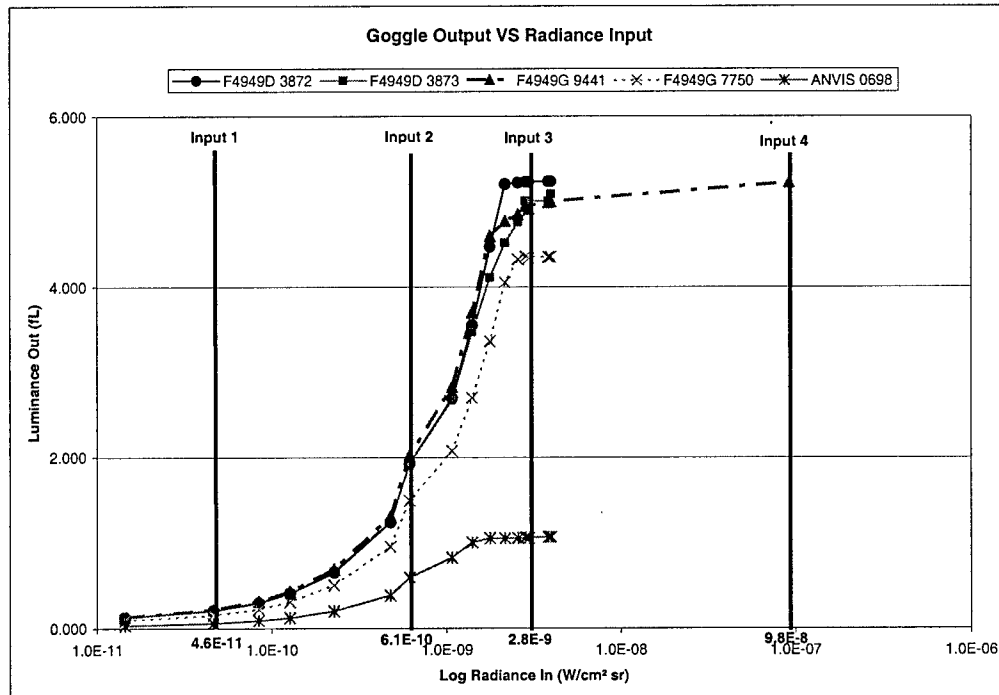
Figure 3. Goggle output luminance vs. radiance input

When the setup was complete and the NVGs and camera were focused, the data collection began. The first study was a comparison of different NVG types. Here, multiple goggles were compared: AN/AVS-6 (Class A minus-blue filter), AN/AVS-9 Model F4949D (unfiltered), AN/AVS-9 F4949D (unfiltered with upgraded tubes), and an AN/AVS-9 F4949G (Class C minus-blue filter). For simplicity, this paper will refer to these goggles as AN/AVS-6, F4949D, F4949D*, and F4949G, respectively. The goggle studied was positioned in the setup and an image of the goggle output was taken. This was repeated for each input radiance. Figure 4, below, shows example images of the NVG at three input radiances. A dark-current image was also taken with the lens cap on the camera lens and a light-blocking blanket covering the camera. Using imaging software, the dark-current image was subtracted from the goggle image. A region of interest (ROI) was then selected to crop out some bad pixels along the edges of the CCD. A histogram was then taken of this ROI and the data sent to a spreadsheet. After the histogram data of the images were stored in a spreadsheet, analysis of the histogram curve was done with curve-fitting software.
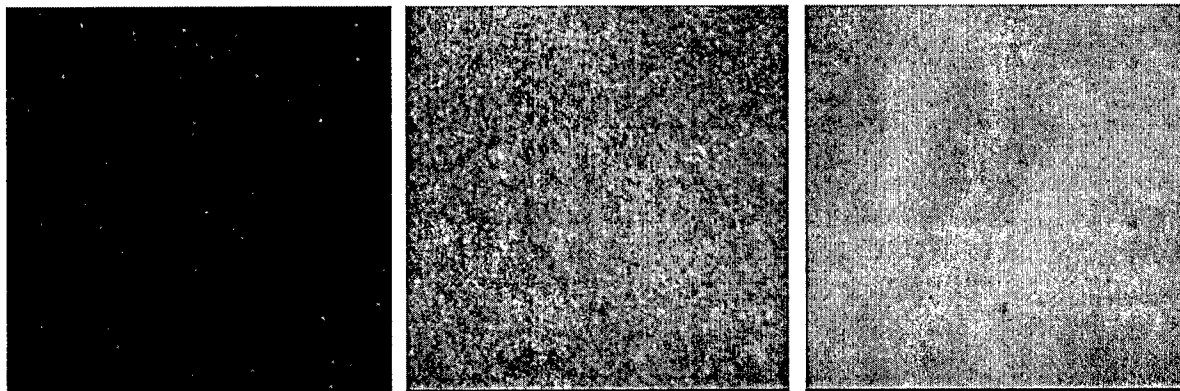

Figure 4. Examples of NVG noise. Input radiance increasing from left to right.

This procedure was repeated to investigate the influence of objective lens filters and eyepiece diopter settings. For the objective lens filter study, a single image intensifier tube and eyepiece were chosen and multiple filters were compared:

no filter, Class A, Class B, Class C. For the eyepiece diopter study, a single goggle was used, and only the diopter setting was varied. Three diopter settings were compared: -1.0, -1.9, -2.8 Diopters (D). For each diopter setting, the camera lens was refocused to compensate. The filters and diopters were studied using the same procedure as the comparison of multiple goggle types. Finally, the procedure from start to finish was repeated three times and multiple images were taken with under the same conditions and using the same goggle to examine the repeatability of the methods used.

3. ANALYSIS

Recall that each NVG noise image was taken with the same CCD camera at the same camera settings and the region of interest was the same. This means that each image contains exactly the same number of pixels and the same pixel depth (10-bit grayscale). Also, the input was a uniform field at a controlled radiance. Histograms of the NVG output noise were plotted for each variable tested. Some hypotheses can be drawn by a quick visual inspection of the histograms and how they differ. For example, a histogram peak centered at a low pixel value represents a darker image than a histogram peak centered at a higher pixel value, described by the Weibull B coefficient. Additionally, a 'taller and thinner' histogram peak represents a smaller range of pixel values (gray levels) within the image and a larger number of pixels at those gray levels, described somewhat by the Weibull A coefficient. A shorter and wider histogram peak represents a larger range of gray levels, characterized by a combination of the Weibull C and D coefficients. The shorter and wider peaks might be attributed to noisier images which will be discussed later.

3.1. Input Radiance

In this section, the response of one NVG will be examined using the four input light conditions. As described above, the input radiances were chosen to cover a wide range of goggle responses ranging from photon-starved to the point where the auto-gain feature of the goggles kicks in. The NVG used in this section is the AN/AVS-9 model F4949D that has been fitted with Upgraded tubes (F4949D*).

First, the noise histograms at the four input levels were examined. Figure 5, below, plots histograms of the F4949D* output at four input radiances. Note that for the lower three input radiances, the profile seems to follow the general characteristic of a Poissonian. However, at the highest radiance, this relationship breaks down. Using a Poisson distribution, one might predict that the histogram of the highest input radiance would follow the trend of decreasing peak amplitude, increasing width, and increasing peak center; however, in reality the fourth peak increases, becomes more narrow, and has only a small change in peak center. This non-Poissionian is most likely due to the effect of the automatic brightness control (ABC) circuit limiting the I^2 tube luminance. Since the ABC limits the luminance, the noise that normally causes the graininess of an NVG image is reduced and the scintillations are seemingly reduced (or at least not as visible). The effects of the ABC are evident both by the naked eye and by the effects on the histogram shown in Figure 5. Visually, the image at the highest brightness seems clearer/cleaner and the scintillations are not as prevalent. The images of the NVG output in Figure 4, above, gives an example of this. In Figure 4, the images are taken at increasing input radiance from left to right. It is easily apparent that the right most image, where the ABC is limiting the output luminance, is less grainy and has less scintillations. Using the histogram data in Figure 4, one can see that the highest input radiance causes the curve to have a higher thinner peak. This higher thinner peak represents a more uniform distribution and possibly a less noisy image. (Note that all four goggles tested behaved similarly for increasing input levels, including the response from the ABC.)
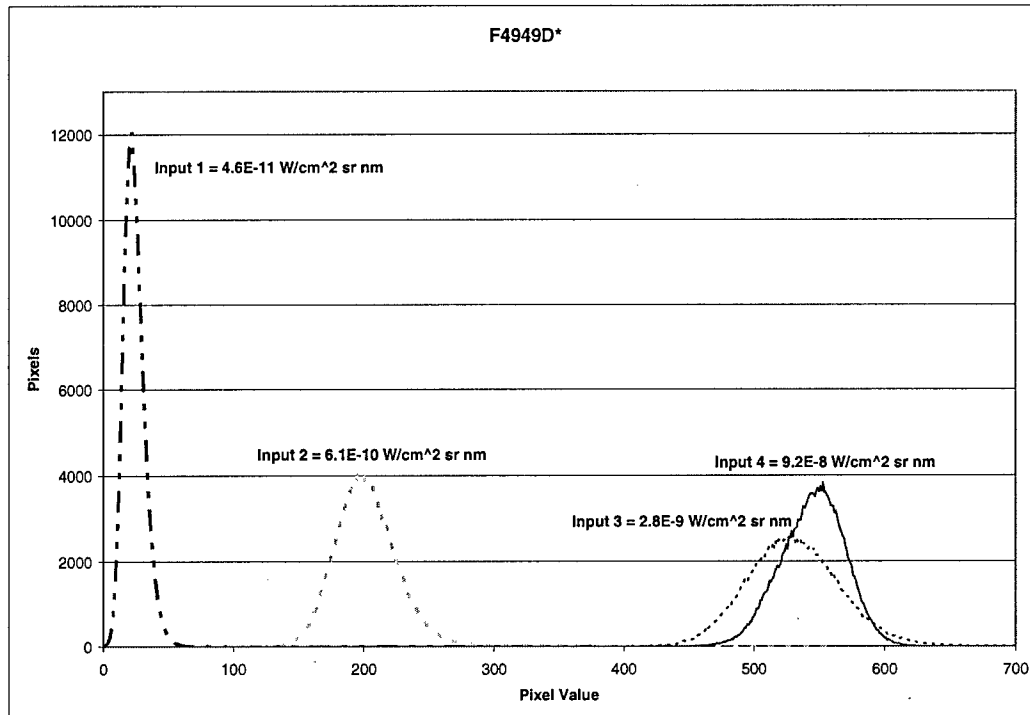
Figure 5. Noise histograms of a single NVG for the four input radiances.

Second, a Weibull distribution curve was fitted to each histogram generating four coefficients, *A-D*, and corresponding 95% confidence levels; see Figures 6-9, below. Note that the 95% confidence levels are plotted as error bars on each graph, but for most points the error bars are smaller than the symbol used to mark the point. Note also that, in general, the error bars for the 95% confidence intervals do not overlap, graphically indicating statistically significant differences between the different measurements. This significance was supported by a more rigorous statistical analysis. However, to avoid filling the paper with reams of data from analyses of variance (ANOVA), the authors have chosen to discuss the statistical significance of the measurements using the graphical representation of the 95% confidence intervals.

In this section, we are going to analyze how the coefficients behave under varying input radiance for each goggle (the next section will examine how the coefficients vary from goggle to goggle). Looking at Figures 6-9, one can see that the coefficients behave similarly for each goggle even though the magnitudes of the coefficients are different for each goggle. In Figure 6, coefficient *A*, which is directly proportional to the histogram peak amplitude, decreased with the first three increasing input radiances and then increased for the fourth input radiance. This trend was the same for every goggle. The behavior of coefficient *A* was similar to a Poissonian distribution (except for the fourth input level) as discussed above. In Figure 7, coefficient *B*, which is directly proportional to the average pixel value/gray level, increased with increasing input radiance and then leveled off for each goggle. The leveling off of coefficient *B* is most likely attributed to the automatic gain control of the goggle. When the gain control of the goggle was engaged, the output luminance of the goggle was limited and therefore limits the maximum gray level of the image. Further increasing the input radiance will not increase the gray level. In Figure 8, coefficient *C* increased with increasing input and then decreased (for most of the NVGs) for the final input level (in the automatic gain control range). The increasing of coefficient *C* means that the histograms curves are getting wider and the back side of the curve more rounded as the input level increases. In Figure 9, coefficient *D* increased with increasing input (for most of the NVGs). Increasing of coefficient *D* means that the curve was getting narrower and the front side of the histogram curve was getting more rounded. The overall effect of coefficients *C* and *D* was to make the histogram curve wider and more rounded on the front and back side.

Finally, one might hypothesize that the scintillations should cause a second and smaller peak to the right of the main peak, resulting in a double peaked distribution or a distribution with a characteristic structure to the right of main body

of the histogram. This distribution would be difficult to model using either the Poisson or Weibull distributions. As seen in Figure 5, the noise measurements made in this effort did not support that hypothesis. This finding will be discussed later in this paper.
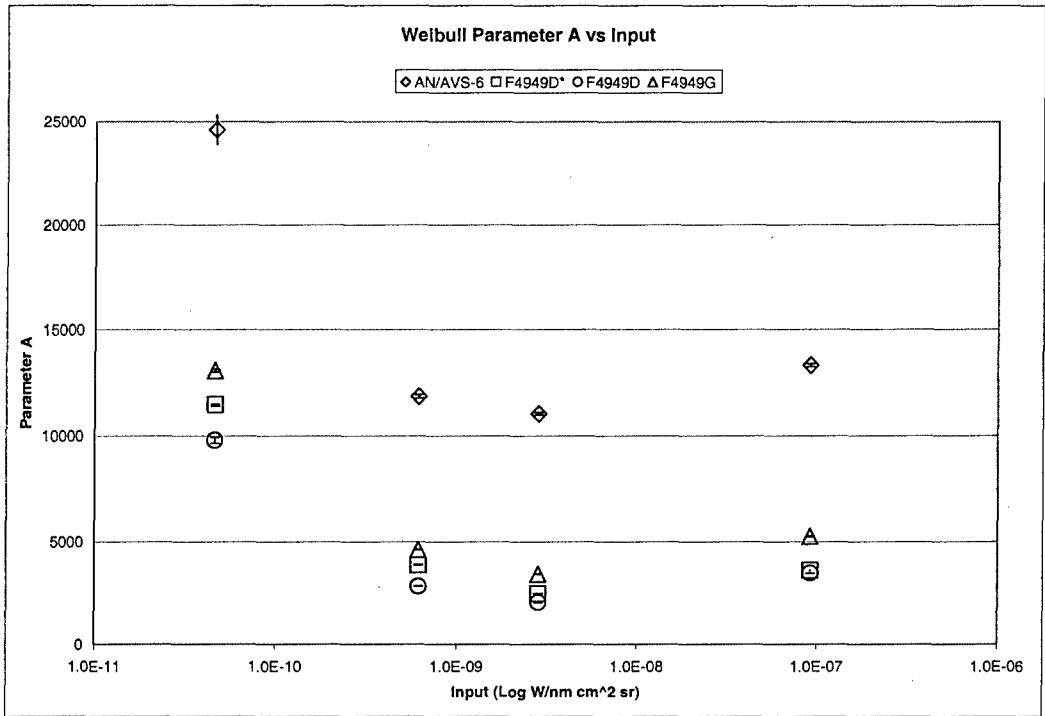
Figure 6. Weibull coefficient A for the four input radiances and for the four NVGs.
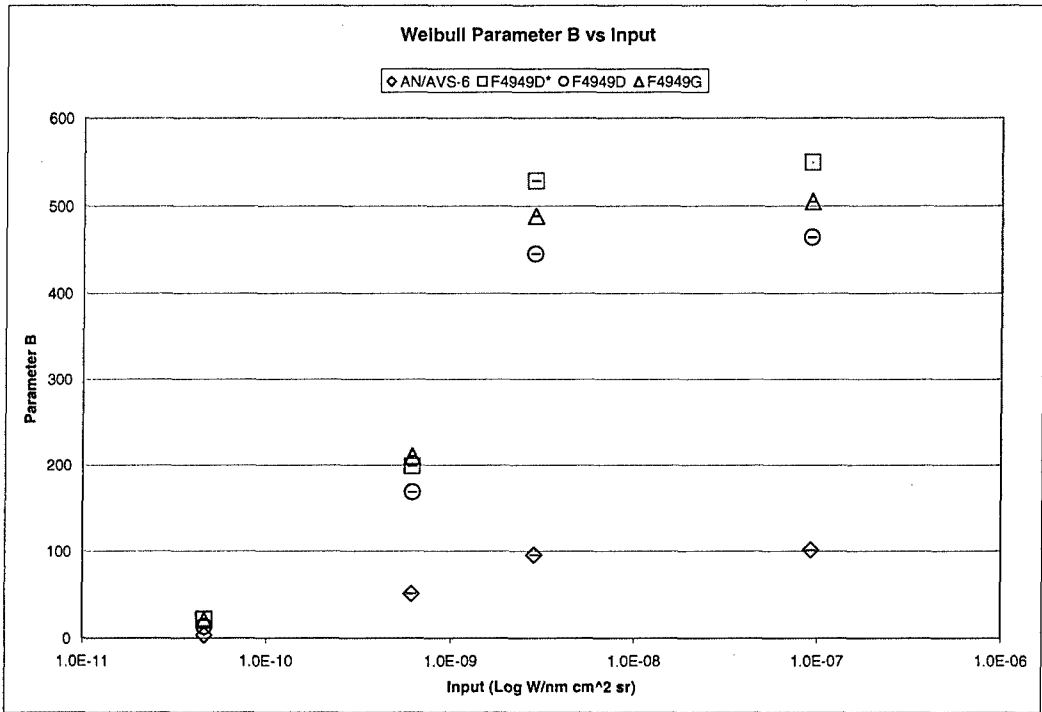
Figure 7. Weibull coefficient B for the four input radiances and for the four NVGs.
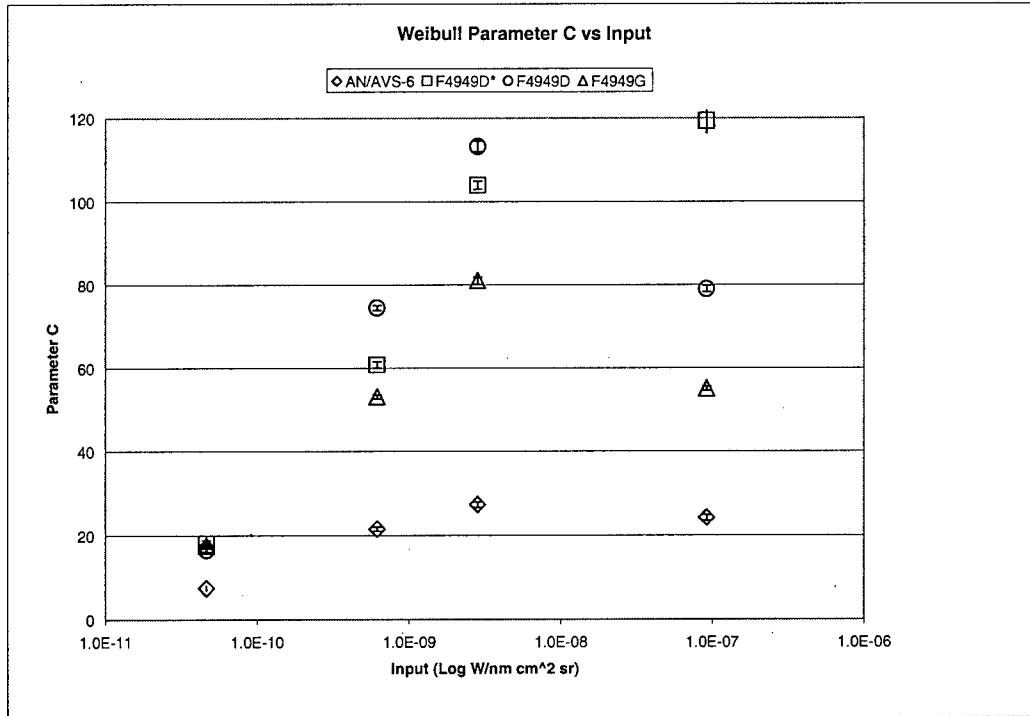
Figure 8. Weibull coefficient C for the four input radiances and for the four NVGs.
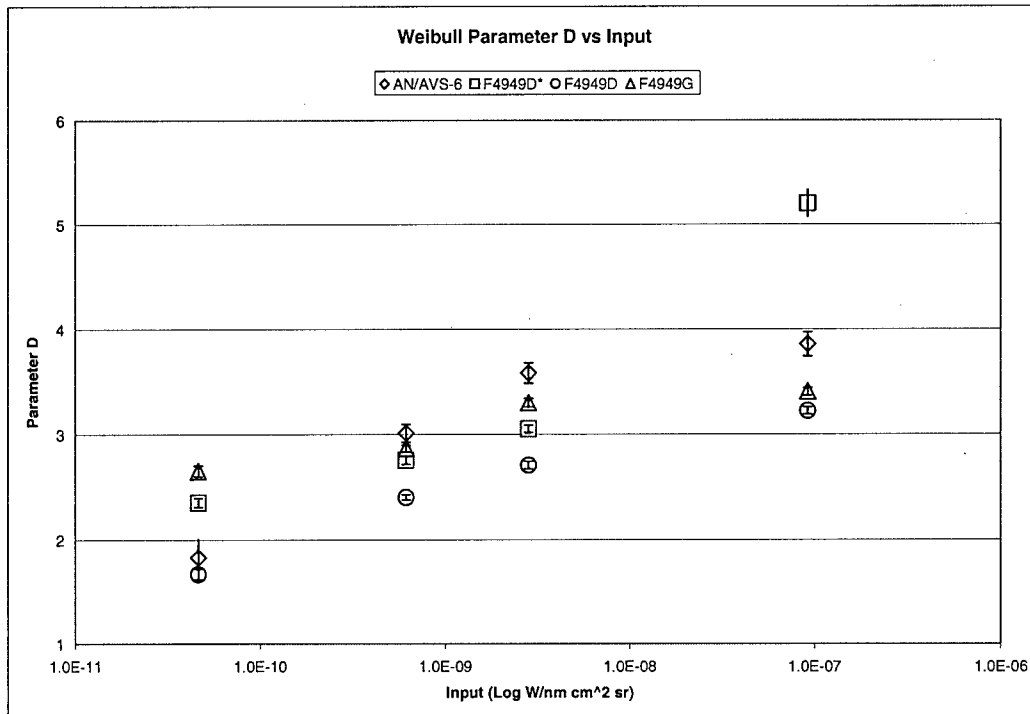

Figure 9. Weibull coefficient D for the four input radiances and for the four NVGs.

3.2. Goggle vs. Goggle

In this section, the responses of the goggles under the various input radiance conditions will be compared with each other. Figure 10, below, shows the histograms of each goggle under the same input light condition. As you can see, each goggle measured seems to have a unique noise histogram. The first obvious difference from goggle to goggle is that the AN/AVS-6 goggle varies drastically from the three other AN/AVS-9 goggles. This is due mostly to the large difference in luminance output of the newer goggles (also depicted in Figure 5). Using the reasoning described earlier that a taller narrower peak corresponds to a less noisy image, then the AN/AVS-6 might be considered to have the least noise of the goggles examined. However, the peak is located to the far left. This means that the image was very dark compared to the other images and that the goggle probably has a lot less gain than the AN/AVS-9's. Comparing the newer goggles to each other, the histograms show that the F4949G has the tallest and thinnest histogram. The F4949D* has a shorter and wider histogram, and the F4949D has the shortest and widest histogram. This trend continued for every other light level tested. The F4949G always had the tallest and thinnest peak except for the AN/AVS-6 which always had a significantly darker image. Another way to say it is that as the tubes get newer, the histogram shifts to the right, indicating higher average luminance output (higher gain). In addition, the oldest tube, the AN/AVS-6, seems to be least noisy at the input radiance level reported below. In addition, there is a significant widening of the histogram when comparing the AN/AVS-6 to the F4949D, the next oldest tube, indicating a significant increase in noise. As the tubes get newer, F4949D* and F4949G, the histograms get narrower, indicating a reduction in overall noise in the newer tubes.

Using the Weibull coefficient plots in Figures 6-9, above, we can infer more about goggle unique noise. The separation of the coefficients from each other tells us that each goggle has a unique noise histogram when compared to other goggles using the same input light conditions. The fact that the 95% confidence intervals do not overlap for most of the input light levels increases the strength of our analysis.
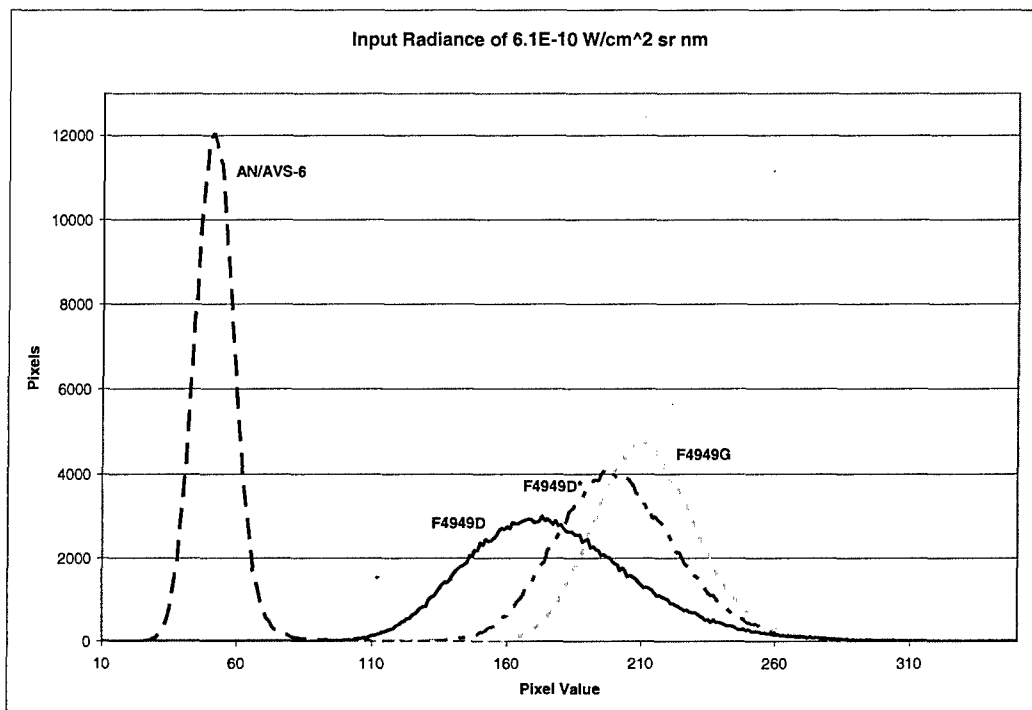

Figure 10. Noise histograms for four NVGs at the same input radiance of 6.1E-10 W/cm^2 sr nm.

3.3. Minus-blue Filters

In this section, the effect of the minus-blue filter on an NVG noise histogram was studied. Here, a single I^2 tube and eyepiece were chosen and objective lenses with four different filters were run through the four input radiances. The filters used were Class A, B, C, and unfiltered objective lenses. Figure 11, below, shows the histograms of the minus-blue filters. Looking closely at the histograms, one can see that the filters generally followed Poissonian-like behavior. The unfiltered NVG allowed more energy to pass through the optics and hit the I^2 tube than the filtered tubes. The unfiltered histogram is slightly shorter and shifted to the right, which is expected from a Poissonian distribution. This was confirmed by examining the Weibull coefficient data for the curves. From Figure 11, one can see that the Class A and un-filtered objective lenses resulted in the 'brightest' peaks and the Class B and Class C filters were less 'bright'. This is an expected result since the unfiltered and Class A objective lenses allow more light and a larger wavelength range to pass through the objective lens to the I^2 tube than the Class B and C filters.
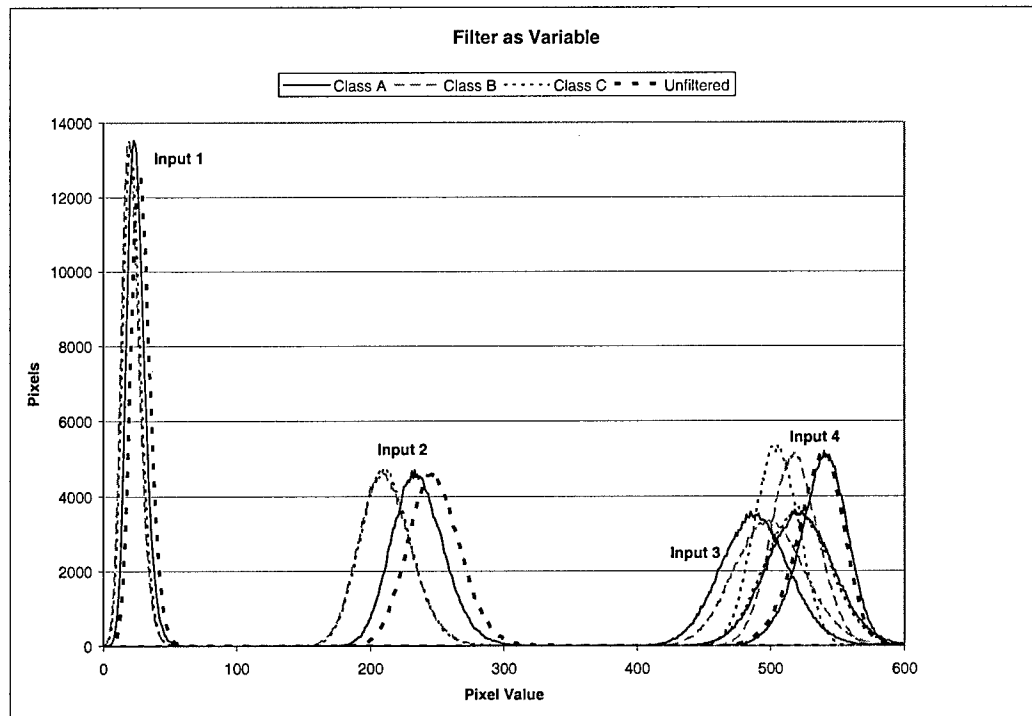
Figure 11. Noise histograms of multiple filters at each of the input radiances (same I^2 and eyepiece used with each filter).

3.4. Eyepiece Diopter Setting

In this section, the effect of eyepiece diopter setting on the image histogram will be examined (see the procedure section above for experiment details). The eyepiece on a NVG has a selectable diopter setting. For all the other variables tested in this paper a diopter setting of -1.0 D was chosen. Theoretically, changing the diopter setting should cause a slight change in magnification (when decreasing the diopter) of the image. This magnification change may affect the apparent noise of a goggle. Here, three diopter settings were studied for one goggle, the F4949G, for three input radiance levels. Diopter settings of -1.0, -1.9, and -2.8 D were chosen. Figure 12, below, is a plot of the image histograms for the three diopter settings studied under three light levels. Figure 12 shows that an increase in negative diopter causes the histogram to be slightly taller, thinner, and 'darker,' shifting to lower average pixel values. This is characteristic of a softening of the image due to defocus. This may be attributed to the magnification of the image 'graininess' spread over more pixels and therefore yielding a narrower range of grey level or a change in the eyepiece Modulation Transfer Function (MTF).
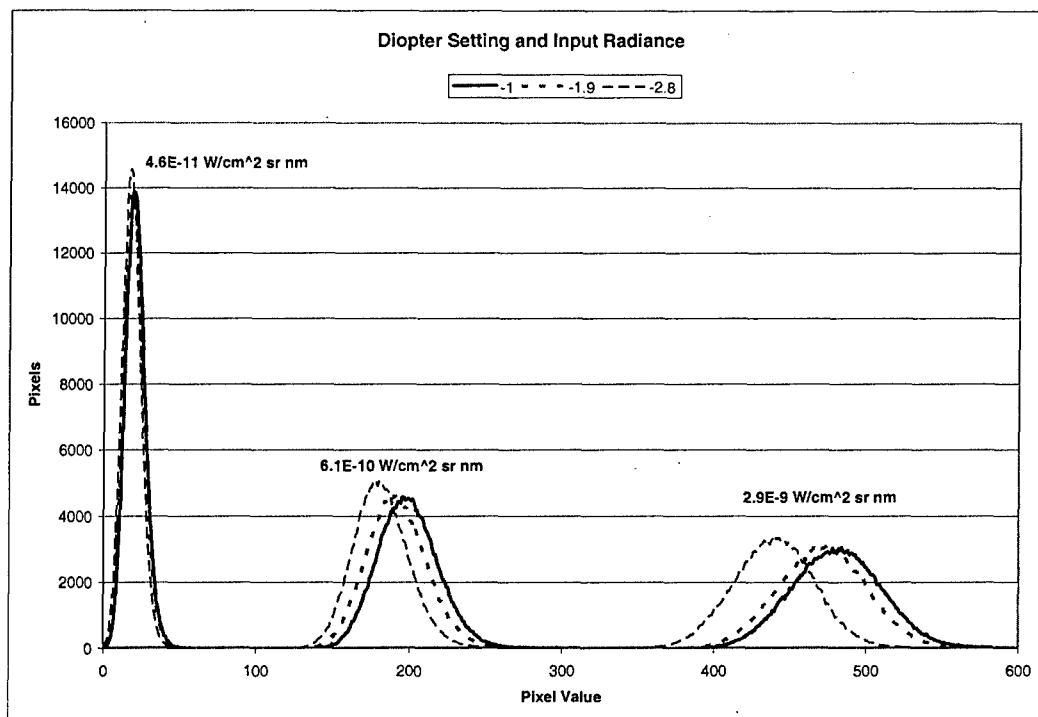
Figure 12. Noise histograms of three eyepiece diopter settings at three of the input radiances (using the same NVG).

4. DISCUSSION

Two noticeable image artifacts had the potential to impact the histograms. The first was the center-to-edge luminance roll-off common in image intensifier tubes. This luminance in the center of the image tube is allowed by manufacturers to be three times that of the edge.[10] This could have a noticeable impact on the noise histograms. The impact might be one of shifting or skewing the histograms to the left, as plotted in this paper, by adding a number of lower or darker pixel values to the histogram. However, the camera used in this experiment had a relatively narrow field of view. This reduced the impact of this roll off on the histograms. A second image artifact that might impact the results of this effort is a fixed pattern resulting from the construction of the fiber optic twist, sometimes referred to as chicken wire. This pattern might add a number of lower or darker pixel values to the histograms, skewing them slightly to favor lower pixel values. The authors found the hexagonal pattern to be very faint. The manufacturing standard limited these brightness deviations to ± 10%.[10] One should keep in mind that the impact on the histogram is unclear and should be studied in greater detail for the sake of completeness. The authors do not anticipate the impact of these two phenomena to be significant enough to change the conclusions of this paper.

The scintillations evident in NVG noise seemed to have little or no impact on the histograms. To the human eye, NVG noise scintillations seem to be points of light that are randomly distributed and are brighter than the background noise. At first glance, the intensity of the scintillations seems to be independent of the input radiance. If anything, visual inspection might conclude that the scintillations are more evident with less input radiance. If this were the case, the scintillations should cause the noise histogram to have a second and smaller peak to the right of the main noise distribution to show that a number of pixels on the CCD contained these scintillations and they were brighter than the rest of the noise. If the scintillations had the same brightness independent from the rest of the noise, the second peak would have been in the same location for each noise level studied. This study did not find a second peak to account for the scintillations. Instead, the scintillations appear to be part of the main noise distribution. In addition, the brightness of the scintillations seems to have about the brightness appropriate to their number and density when compared to the majority of the noise distribution.

This approach is probably only comparable to other measurements made using the same equipment, procedure, and settings, given the number of degrees of freedom. Equipment changes yielded noticeable changes in the Weibull coefficients. Considerable effort was made to achieve consistent data. The approach might have been improved by a lower noise floor camera with greater dynamic range. A CCD with smaller pixels and more sensitivity might be able to resolve certain aspects of the noise better, such as the scintillations, but would also stray from the capabilities of the human eye. The results may be different if a larger lens system was used to capture more of the NVG image.

5. CONCLUSION

This approach to measuring the spatial nature of NVG noise seemed to work well. One objective of this study was to determine if a statistical difference between goggles' noise histograms could be measured. The confidence intervals suggest that it is relatively easy to get statistically significant differences between noise distributions (Weibull fits). Since we were able to show a separation of coefficients for each goggle, we believe that a statistical difference exists. Further examination of the spatial nature of NVG noise is needed to narrow down the parameters that contribute to this statistical difference.

This study found that external factors have a significant impact on spatial noise distribution. Some of these factors were predicted, such as the effect of the input radiance on the noise distribution. Other factors such as how the goggle eyepiece setting and minus blue filter affected the noise distribution where not as easily predictable. These two variables do have an impact on the noise distribution and may have been an unknown factor in the visually perceived noise studies mentioned in the introduction[1,3,4]. For example, a subject that dials in a large negative diopter to correct for their vision will also be shifting the mean pixel value of the noise distribution. This change might affect the way the subject rates the NVG noise.

Another conclusion drawn from this study was that newer tubes seem to be less noisy than older tubes. This study compared several goggles of varying ages and tube technology. The newest and most recent of I^2 tube technology (the Upgraded tube) seemed to have the best noise distribution. The newer tube distribution had a taller and narrower peak that corresponds to a narrower range of pixel values which is what one would expect if less noise were present.

6. ACKNOWLEDGEMENTS

7. REFERENCES

1. Glasgow, R.L., Marasco, P.L., Havig, P.R., Martinsen, G.L., Reis, G.A., & Heft, E.L., "Psychophysical measurement of night vision goggle noise", in *Helmet- and Head-Mounted Displays XIII: Technologies and Applications*, edited by Clarence E. Nash, Colin E. Reese, Proceedings of SPIE Vol. 5079 (SPIE, Bellingham, WA, 2003) 164-173.

2. Rivamonte, A. "Resolution and signal-to-noise measurement U.S. Army night vision goggles", in *Helmet-Mounted Displays II*, edited by R.J. Lewendowski, Proceedings of SPIE Vol. 1290, pp. 206-215, SPIE, Orlando, FL, 1990.

3. Reis, G.A., Marasco, P.L., Havig, P.R., & Heft, E.L., "Psychophysical measurement of night vision goggle noise using a binocular display", in *Helmet- and Head-Mounted Displays IX: Technologies and Applications*, edited by Clarence E. Nash, Colin E. Reese, Proceedings of SPIE Vol. 5442 (SPIE, Bellingham, WA, 2004) 13-24.

4. Reis, George A, Marasco, Peter L., Havig, Paul R., Heft, Eric L., & Goodyear, Charles D., "Characterizing night vision goggle noise using the method of paired comparisons", in *Helmet- and Head-Mounted Displays X: Technologies and Applications*, edited by Clarence E. Nash, Colin E. Reese, Proceedings of SPIE Vol. 5800 (SPIE, Bellingham, WA, 2005) 9-20.

5. Pinkus, A.R., 1991. *Night Vision Goggle Ambient Illumination Testing*, US Patent #5,070,239.

6.   Dereniak, E.L., Crow, D.G., *Optical Radiation Detectors*, John Wiley and Sons, New York, 1984.

7.   Bell, R.L., "Noise figure of the MCP image intensifier tube," *IEEE Transactions on Electron Devices*, Vol. ED-22, No. 10, October 1975.

8.   Angel, S. D. & Baldwin, J. B., "Aircrew visual acuity viewing with different night vision goggle eyepiece diopter settings", in *Helmet- and Head-Mounted Displays IX: Technologies and Applications*, edited by Clarence E. Nash, Colin E. Reese, Proceedings of SPIE Vol. 5442 (SPIE, Bellingham, WA, 2004) 1-12.

9.   Marasco, P.L. & Task, H. L., "The Impact of Target Luminance and Radiance on Night-Vision Device Visual Performance Testing", in *Helmet- and Head-Mounted Displays XIII: Technologies and Applications*, edited by Clarence E. Nash, Colin E. Reese, Proceedings of SPIE Vol. 5079 (SPIE, Bellingham, WA, 2003) 174-183.

10. Military Specification, *Image Intensifier Assembly, 18mm, Microchannel Wafer MX-10160/AVS-6*, MIL-I-49428(CR), 1989, 8-9.
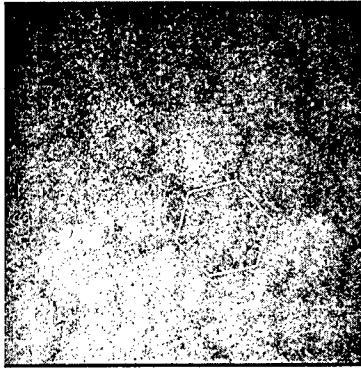
Figure 20. Fiber bundles distinguishable (see white outline example); here contrast is adjusted to see them easier.

Weibull Coeff.	Input Radiance (W/cm^2 nm sr)	NVG	Coeff. Value	95% Confidence Lower	95% Confidence Upper
Param A					
	4.6E-11				
		AN/AVS-6	24607.14	23892.22	25322.05
		F4949D*	11474.64	11395.49	11553.79
		F4949D	9798.76	9657.89	9939.62
		F4949G	13068.54	12992.62	13144.45
	6.1E-10				
		AN/AVS-6	11853.44	11767.80	11939.07
		F4949D*	3887.28	3870.31	3904.26
		F4949D	2851.95	2841.51	2862.39
		F4949G	4620.31	4605.80	4634.82
	2.8E-09				
		AN/AVS-6	11037.10	10977.58	11096.62
		F4949D*	2501.14	2494.13	2508.14
		F4949D	2064.76	2056.55	2072.97
		F4949G	3442.67	3433.46	3451.89
	9.2E-08				
		AN/AVS-6	13311.02	13238.64	13383.40
		F4949D*	3621.56	3610.30	3632.82
		F4949D	3485.39	3477.01	3493.77
		F4949G	5258.64	5246.47	5270.81

Param B		NVG	Coeff. Value	95% Confidence Lower	95% Confidence Upper
	4.6E-11				
		AN/AVS-	3.60	3.34	3.86

	NVG	Coeff. Value	95% Confidence Lower	95% Confidence Upper
	6			
	F4949D*	21.85	21.76	21.93
	F4949D	13.66	13.35	13.96
	F4949G	20.89	20.82	20.95
6.1E-10				
	AN/AVS-6	51.18	51.10	51.27
	F4949D*	198.93	198.77	199.09
	F4949D	168.71	168.52	168.90
	F4949G	210.50	210.40	210.59
2.8E-09				
	AN/AVS-6	95.45	95.38	95.52
	F4949D*	528.59	528.43	528.75
	F4949D	445.24	444.96	445.52
	F4949G	488.40	488.29	488.51
9.2E-08				
	AN/AVS-6	101.42	101.36	101.48
	F4949D*	549.47	549.36	549.59
	F4949D	464.12	464.02	464.22
	F4949G	504.72	504.66	504.78

Param C	NVG	Coeff. Value	95% Confidence Lower	95% Confidence Upper
4.6E-11				
	AN/AVS-6	7.52	6.95	8.09
	F4949D*	18.09	17.83	18.34
	F4949D	16.62	16.28	16.96
	F4949G	17.64	17.37	17.92
6.1E-10				
	AN/AVS-6	21.55	21.02	22.08
	F4949D*	60.90	60.13	61.66
	F4949D	74.51	73.92	75.10
	F4949G	53.20	52.68	53.72
2.8E-09				
	AN/AVS-6	27.30	26.62	27.97
	F4949D*	104.01	102.99	105.03
	F4949D	113.28	112.03	114.54
	F4949G	81.04	80.17	81.91
9.2E-08				
	AN/AVS-6	24.25	23.57	24.93
	F4949D*	119.34	116.45	122.24
	F4949D	79.07	78.33	79.80

		F4949G	55.19	54.65	55.73

Param D		NVG	Coeff. Value	95% Confidence Lower	95% Confidence Upper
	4.6E-11				
		AN/AVS-6	1.83	1.66	2.00
		F4949D*	2.36	2.31	2.40
		F4949D	1.67	1.62	1.72
		F4949G	2.65	2.60	2.70
	6.1E-10				
		AN/AVS-6	3.01	2.93	3.10
		F4949D*	2.76	2.72	2.80
		F4949D	2.41	2.38	2.43
		F4949G	2.87	2.84	2.90
	2.8E-09				
		AN/AVS-6	3.58	3.49	3.68
		F4949D*	3.05	3.02	3.09
		F4949D	2.71	2.67	2.75
		F4949G	3.30	3.26	3.34
	9.2E-08				
		AN/AVS-6	3.86	3.74	3.97
		F4949D*	5.20	5.08	5.33
		F4949D	3.22	3.19	3.26
		F4949G	3.41	3.37	3.44

Radiance	Diopter	Value	-	+
4.60E-11	Class A	13266.91757	71.96345	71.96345
6.10E-10	Class A	4497.492076	14.56257	14.56257
2.80E-09	Class A	3488.104713	10.097231	10.097231
9.20E-08	Class A	5008.060673	14.042594	14.042595
4.60E-11	Class B	13237.94056	84.25479	84.25478
6.10E-10	Class B	4516.630869	15.499411	15.499411
2.80E-09	Class B	3312.415939	8.784573	8.784573
9.20E-08	Class B	4997.326775	18.751382	18.751383
4.60E-11	Class C	13068.53604	75.91109	75.91108
6.10E-10	Class C	4620.307585	14.508649	14.508649
2.80E-09	Class C	3442.673472	9.21633	9.216329
9.20E-08	Class C	5258.639089	12.169106	12.169105
4.60E-11	Unfiltered	12379.12971	67.1002	67.10019
6.10E-10	Unfiltered	4486.337187	17.481112	17.481112
2.80E-09	Unfiltered	3558.482127	8.93134	8.931339
9.20E-08	Unfiltered	5044.22868	12.076379	12.076379

Radiance	Filter	Value	-	+
4.6E-11	Class A	23.44009586	0.0602551	0.0602551

			-	+
6.1E-10	Class A	233.9369505	0.1035208	0.1035208
2.8E-09	Class A	522.2293008	0.1166901	0.1166901
9.2E-08	Class A	542.0887196	0.0770607	0.0770606
4.6E-11	Class B	19.53295148	0.0709655	0.0709655
6.1E-10	Class B	209.5082898	0.1095448	0.1095447
2.8E-09	Class B	498.9169986	0.113763	0.1137631
9.2E-08	Class B	517.6943572	0.1071022	0.1071022
4.6E-11	Class C	20.885331	0.0647124	0.0647124
6.1E-10	Class C	210.4971902	0.0973756	0.0973756
2.8E-09	Class C	488.3967261	0.1096965	0.1096966
9.2E-08	Class C	504.721611	0.0625588	0.0625587
4.6E-11	Unfiltered	27.42203947	0.0633422	0.0633422
6.1E-10	Unfiltered	246.7433595	0.1237045	0.1237045
2.8E-09	Unfiltered	520.5291256	0.099585	0.0995851
9.2E-08	Unfiltered	539.8758358	0.0652896	0.0652895

Radiance	Filter	Value	-	+
4.60E-11	Class A	16.38752286	0.2091693	0.2091693
6.10E-10	Class A	53.8508619	0.5245596	0.5245596
2.80E-09	Class A	81.55243273	0.9823906	0.9823906
9.20E-08	Class A	82.76629696	1.7301142	1.7301141
4.60E-11	Class B	16.48871537	0.2480827	0.2480826
6.10E-10	Class B	52.37367267	0.513811	0.513811
2.80E-09	Class B	80.30421787	0.7769091	0.7769091
9.20E-08	Class B	52.99727483	0.7150891	0.7150891
4.60E-11	Class C	17.6412637	0.274194	0.274194
6.10E-10	Class C	53.19776424	0.5202517	0.5202517
2.80E-09	Class C	81.04160174	0.8694782	0.8694782
9.20E-08	Class C	55.1859398	0.5393487	0.5393487
4.60E-11	Unfiltered	18.98405722	0.2871035	0.2871035
6.10E-10	Unfiltered	56.4511742	0.7320029	0.7320029
2.80E-09	Unfiltered	80.03865877	0.8319753	0.8319753
9.20E-08	Unfiltered	92.38565809	1.9212058	1.9212058

Radiance	Filter	Value	-	+
4.60E-11	Class A	2.487182192	0.0397729	0.0397729
6.10E-10	Class A	2.817027875	0.0322907	0.0322907
2.80E-09	Class A	3.376077235	0.0448918	0.0448918
9.20E-08	Class A	5.029802444	0.1083524	0.1083524
4.60E-11	Class B	2.492714309	0.0469272	0.0469272
6.10E-10	Class B	2.745280809	0.0320673	0.0320673
2.80E-09	Class B	3.126017533	0.0341813	0.0341813
9.20E-08	Class B	3.100763849	0.0474183	0.0474183
4.60E-11	Class C	2.654306217	0.0499328	0.0499328
6.10E-10	Class C	2.868148192	0.0327524	0.0327524
2.80E-09	Class C	3.300963267	0.039345	0.039345
9.20E-08	Class C	3.406427365	0.0366592	0.0366592
4.60E-11	Unfiltered	2.716118217	0.0491717	0.0491717

			-	+
6.10E-10	Unfiltered	2.971120858	0.0443512	0.0443512
2.80E-09	Unfiltered	3.366370089	0.038657	0.038657
9.20E-08	Unfiltered	5.664353444	0.120184	0.120184

Radiance	Diopter	Value A	-	+
4.6E-11	-1	13628.06683	64.82221	64.8222
4.7E-11	-1.9	13675.95121	102.62603	102.62602
4.6E-11	-2.8	14160.4539	106.2363	106.2363
6.1E-10	-1	4488.237908	11.513136	11.513136
6.1E-10	-1.9	4466.808948	13.636851	13.63685
6.0E-10	-2.8	4936.343245	21.920493	21.920494
2.8E-09	-1	2972.925077	6.107024	6.107025
2.8E-09	-1.9	3032.240544	6.776995	6.776995
2.8E-09	-2.8	3290.770751	8.322997	8.322997

Radiance	Diopter	Value B	-	+
4.6E-11	-1	19.6669587	0.051019	0.051019
4.6E-11	-1.9	18.80760651	0.0797964	0.0797964
4.6E-11	-2.8	17.57634557	0.0772239	0.0772239
6.1E-10	-1	197.5770598	0.0821235	0.0821236
6.1E-10	-1.9	190.3703642	0.0967233	0.0967234
6.1E-10	-2.8	179.9571944	0.1292036	0.1292036
2.8E-09	-1	481.3278512	0.0978833	0.0978833
2.8E-09	-1.9	472.6519357	0.1038147	0.1038148
2.8E-09	-2.8	440.9652907	0.1076553	0.1076553

Radiance	Diopter	Value C	-	+
4.6E-11	-1	16.30648927	0.1899158	0.1899158
4.6E-11	-1.9	16.36726759	0.307703	0.307703
4.6E-11	-2.8	16.21060362	0.3251452	0.3251452
6.1E-10	-1	55.15454744	0.4441189	0.4441189
6.1E-10	-1.9	55.1391848	0.5277822	0.5277822
6.1E-10	-2.8	48.5603192	0.6371311	0.6371311
2.8E-09	-1	97.2566223	0.8435433	0.8435433
2.8E-09	-1.9	98.63076975	0.9921013	0.9921013
2.8E-09	-2.8	93.89584239	1.1348985	1.1348985

Radiance	Diopter	Value D	-	+
4.6E-11	-1	2.548774762	0.0367316	0.0367316
4.6E-11	-1.9	2.57804406	0.0596033	0.0596033
4.6E-11	-2.8	2.645605304	0.0642927	0.0642927
6.1E-10	-1	2.880069527	0.0270326	0.0270326
6.1E-10	-1.9	2.888903244	0.0321915	0.0321915
6.1E-10	-2.8	2.791538358	0.0432755	0.0432755
2.8E-09	-1	3.405885753	0.0325296	0.0325296
2.8E-09	-1.9	3.542581963	0.0388439	0.0388439
2.8E-09	-2.8	3.679924269	0.0480577	0.0480577

W-coeff	NVIS_B	Class A	Class B	Class C	Unfiltered	avg	stdev	stdev%	W-coeff	Max
A	4.60E-11	13266.91757	13237.94056	13068.53604	12379.12971	12988.13097	415.3208838	3.2%	A	13266.91
A	6.10E-10	4497.492076	4516.630869	4620.307585	4486.337187	4530.191929	61.36571406	1.4%	A	4620.307
A	2.80E-09	3488.104713	3312.415939	3442.673472	3558.482127	3450.419063	103.6061299	3.0%	A	3558.482
A	9.20E-08	5008.060673	4997.326775	5258.639089	5044.22868	5077.063804	122.7017459	2.4%	A	5258.639
B	4.60E-11	23.44009586	19.53295148	20.885331	27.42203947	22.82010445	3.469434067	15.2%	B	27.42203
B	6.10E-10	233.9369505	209.6082898	210.4971902	246.7433595	225.1714475	18.28341477	8.1%	B	246.7433
B	2.80E-09	522.2293008	498.9169986	488.3967261	520.5291256	507.5180378	16.58626039	3.3%	B	522.2293
B	9.20E-08	542.0887196	517.6943572	504.721611	539.8758358	526.0951309	18.01021061	3.4%	B	542.0887
C	4.60E-11	16.38752286	16.48871537	17.6412637	18.98405722	17.37538979	1.213888028	7.0%	C	18.98405
C	6.10E-10	53.8508619	52.37367267	53.19776424	56.4511742	53.96836825	1.762102689	3.3%	C	56.4511
C	2.80E-09	81.55243273	80.30421787	81.04160174	80.03865877	80.73422778	0.691053028	0.9%	C	81.55243
C	9.20E-08	82.76629696	52.99727483	55.1859398	92.38565809	70.83379242	19.74727179	27.9%	C	92.38565
D	4.60E-11	2.487182192	2.492714309	2.654306217	2.716118217	2.587580234	0.115547509	4.5%	D	2.716118
D	6.10E-10	2.817027875	2.745280809	2.868148192	2.971120858	2.850394434	0.094960109	3.3%	D	2.971120
D	2.80E-09	3.376077235	3.126017533	3.300963267	3.366370089	3.292357031	0.115801412	3.5%	D	3.376077
D	9.20E-08	5.029802444	3.100763849	3.406427365	5.664353444	4.300336776	1.242405043	28.9%	D	5.664353